AIAA JOURNAL
Vol. 30, No. 10, October 1992

Numerical Study of Film Cooling in Supersonic Flow

John P. O'Connor* and A. Haji-Sheikh†
University of Texas at Arlington, Arlington, Texas 76019

A computational fluid dynamics study of the insulating effects of film cooling is presented. The results for injecting a heated secondary airstream through a rearward-facing slot into a supersonic primary stream are compared with experimental data. The secondary stream is injected parallel to a flat plate in a Mach 3.0 divergent nozzle. Three different slot openings are examined. The secondary-air-flow to primary-air-flow ratio is between 0.5 and 8%.

Nomenclature

C_p = specific heat
H = step height
M = secondary-to-primary mass velocity ratio, $(\rho U)_s/(\rho U)_p$
Ma = Mach number
Pr = Prandtl number
r = recovery factor
S = slot height
T_{aw} = local adiabatic wall temperature
T_{aw2} = adiabatic wall temperature at injection point
T_∞ = local primary static temperature
T_o = primary total temperature
T_r = recovery temperature
TR = secondary-to-primary total temperature ratio
U = local primary flow velocity
W = flow rate
X = axial distance downstream from injection point
X_1 = axial distance downstream from injection point for near ideal film cooling ($\eta > 0.95$)
ρ = density, kg/m^3
η = film-cooling effectiveness
μ = fluid kinematic viscosity

Subscripts

p = primary flow
s = secondary flow

Introduction

In many engineering applications, there is a need to protect solid surfaces that are exposed to a high-temperature environment. The aerospace industry specifically has been addressing this problem for years. Hypersonic vehicles are exposed to a gaseous high-temperature environment and their solid surfaces must be cooled or manufactured from special high-temperature materials. Components of gas turbine engines are exposed to high-temperature gases. The thrust produced by these engines is limited by turbine blade material temperature limits; therefore, it is desirable to cool the blades. Exhaust system surfaces of high-performance jet aircraft are subject to high-temperature exhaust gases. There is a need to cool these surfaces for material survivability and infrared signature reduction. There are many other current and future applications as well.

Presented as Paper 91-4010 at the National Heat Transfer Conference, Minneapolis, MN, July 28–31, 1991; received Aug. 28, 1991; revision received March 14, 1992; accepted for publication March 14, 1992.

*Graduate Student, Department of Mechanical Engineering.
†Professor, Department of Mechanical Engineering. Member AIAA.

Film cooling is one way of introducing a coolant air flow into a boundary layer. A secondary fluid is injected through a slot or series of holes at one or more discrete locations along a surface with the objective of insulating that surface not only in the immediate region of the point of injection, but also downstream of that point. The secondary fluid feeds downstream from the injection point, creating an insulating film that reduces the convective heat transfer rate from the hot gas stream to the exposed surface. Seban et al.[1] investigated the effect of secondary coolant fluid injection angularity on film-cooling effectiveness and found that, as the secondary injection angle with respect to the primary flow stream increases, film-cooling effectiveness decreases. Secondary injection normal to the primary stream resulted in up to a 50% reduction in cooling effectiveness. As the injection angle increases, mixing between the two streams increases. Mixing tends to break down the insulating film and is not desired. The highest effectiveness values were obtained when the secondary coolant fluid was injected parallel to the primary stream, a flow condition where mixing is at a minimum. Hence, this computational study was based on a geometry where the secondary airflow injection was parallel to the primary stream.

The coolant airflow can be injected through holes or slots and at different angles with respect to the primary flow stream. The primary flow stream to which the coolant fluid is injected can be subsonic or supersonic. The technique used depends on the specific application. This study addresses film cooling in a supersonic environment. Studies of transpiration cooling and other different film-cooling techniques are widely reported in the literature. A discussion on transpiration cooling can be found in Ref. 2 and various film-cooling techniques are discussed in Refs. 3–7. In addition, Ref. 7 includes a survey of film-cooling studies reported by Goldstein.

Objectives

The objectives of this study are twofold: 1) to verify the numerical model, and 2) to generate a data base using computational tools that improve the design and analysis capabilities of supersonic film-cooling applications. Computational tools are very useful in examining a flowfield in detail; this capability is used to provide a qualitative explanation of the parameters affecting film cooling. These parameters include mass velocity ratio, flowfield properties, slot and step geometry, axial location, and fluid injection angle.

The present study focuses on injecting a heated film of air through a rearward-facing slot parallel to a flat plate in a Mach 3 divergent nozzle. The specific geometry studied was taken from the work of Goldstein et al.[3] Three different slot heights, S = 1.62, 3.12, and 4.62 mm, are analyzed. Six secondary airflow values are selected for each slot height, resulting in secondary-to-primary airflow ratios between 0.5 and 8%.

Film cooling is dependent on several parameters. The scope of the current study is limited by analyzing a single tempera-

ture ratio where the total temperature of the primary flow is 297 K and the total temperature of the secondary flow is 366 K, resulting in a temperature ratio of 1.23. Note that the secondary gas is at a higher temperature than the primary gas. This study might be more appropriately labeled as film heating; however, for this temperature ratio, the flow can be considered constant property. Under these conditions, the dimensionless temperature distribution in the boundary layer is independent of whether the secondary gas is at a higher or lower temperature than the primary gas.

Geometry Definitions

The geometry on which this study is based is illustrated in Fig. 1 and was taken from Ref. 3, which contains experimental results. Goldstein et al.[3] used a constant width of 63.5 mm so that three-dimensional effects were minimized. The numerical data generated from this study are for a two-dimensional flow. The sonic throat height is 5.94 mm, resulting in a throat area of 378.1 mm^2. At the point of secondary fluid injection, the primary flow area is 1095 mm^2 resulting in a local-to-sonic throat expansion area ratio of 2.89. Between the sonic throat location and the point of secondary fluid injection (approximately 79.25 mm), primary flow expands along a flat plate on the bottom surface and along a top surface designed to provide isentropic expansion. This is to prevent the formation of shock waves upstream of the secondary fluid injection point. The test section begins at the secondary fluid injection point or mixing plane. The mixing plane identifies the cross section of the test apparatus at which the secondary and primary flows merge. At this location, the bottom surface encounters an abrupt step down. A 1.45-mm-thick splitter plate separates the two flow streams. Secondary flow slot heights of $S = 1.62$, 3.12, and 4.62 mm are investigated, resulting in three step heights $H = 3.07$, 4.57, and 6.07 mm, respectively. The step height is the sum of the slot height and splitter-plate thickness t. The surface on which the temperature distribution is desired is a flat plate that extends 225.42 mm downstream from the secondary fluid injection point or mixing plane. The maximum cross-sectional area of the primary flow is 1767.7 mm^2 corresponding to an overall expansion area ratio of 4.69.

Figure 1 illustrates the location of the primary and secondary flow streams and the surface that is to be film cooled. Primary flow total temperature and pressure are 297 K and 0.276 MPa, respectively, for all analyses conducted. At the secondary injection point or mixing plane, the local Mach number of the primary flow is 2.24. The local Reynolds number of the primary flow at the edge of the splitter plate based on local conditions and primary flow passage height is 4.4×10^5, indicating a laminar boundary layer. As the primary flow moves aft of the mixing plane, it expands to a Mach number of 3.1.

Table 1 shows the secondary flow conditions corresponding to the 3.07-mm step height. Secondary total pressure P_s and flow rate W_s are given along with the secondary-to-primary airflow ratio W_s/W_p, mass velocity ratio M, secondary slot Mach number Ma_s, and the mixing plane velocity ratio U_s/U_p. Secondary flow conditions for the 4.57- and 6.07-mm step heights are tabulated in Tables 2 and 3, respectively.

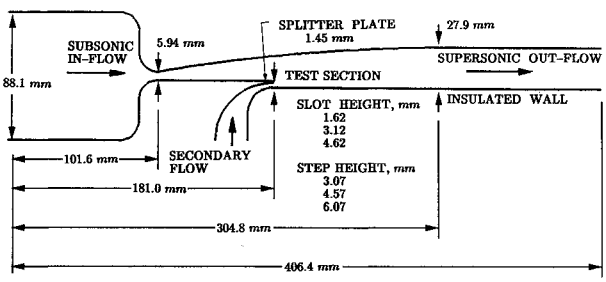

Fig. 1 Geometry and flow information.

Table 1 Secondary flow conditions for $H = 3.07$ mm

CFD[a] run	P_s, kPa	W_s, kg/min	W_s/W_p	M	Ma_s	U_s/U_p
1	15.17	0.130	0.0088	0.094	0.43	0.296
2	20.68	0.241	0.0164	0.174	0.75	0.497
3	27.58	0.340	0.0232	0.245	0.96	0.618
4	34.47	0.427	0.0291	0.309	1.06	0.674
5	44.81	0.558	0.0381	0.403	1.13	0.705
6	55.16	0.688	0.0469	0.497	1.16	0.719

[a]CFD = computational fluid dynamics.

Table 2 Secondary flow conditions for $H = 4.57$ mm

CFD[a] run	P_s, kPa	W_s, kg/min	W_s/W_p	M	Ma_s	U_s/U_p
1	10.58	0.101	0.0069	0.038	0.23	0.158
2	13.79	0.199	0.0135	0.075	0.36	0.250
3	18.34	0.392	0.0267	0.147	0.64	0.432
4	21.17	0.493	0.0336	0.185	0.79	0.525
5	27.85	0.676	0.0461	0.254	1.00	0.642
6	35.85	0.873	0.0595	0.328	1.08	0.683

[a]CFD = computational fluid dynamics.

Table 3 Secondary flow conditions for $H = 6.07$ mm

CFD[a] run	P_s, kPa	W_s, kg/min	W_s/W_p	M	Ma_s	U_s/U_p
1	10.58	0.150	0.0102	0.038	0.23	0.159
2	15.31	0.399	0.0272	0.101	0.46	0.320
3	17.93	0.561	0.0383	0.142	0.62	0.420
4	21.17	0.737	0.0502	0.187	0.79	0.527
5	25.51	0.922	0.0629	0.234	0.96	0.621
6	30.34	1.110	0.0757	0.282	1.05	0.667

[a]CFD = computational fluid dynamics.

For all secondary flow conditions, the Reynolds number based on secondary flow sonic conditions and slot height is on the order of 10^4, indicating a laminar boundary layer at the mixing plane. When the two parallel streams meet downstream of the splitter plate, a separated region forms and turbulent mixing is initiated.[8] A turbulent boundary layer exists on the surface of interest downstream from the injection point.

Computational Approach

The conservation equations for mass, momentum, and energy form the cornerstone of theoretical fluid dynamics. These equations describe the variations of fluid pressure, temperature, density, velocity, and other flowfield properties throughout space and time. Computational fluid dynamics (CFD) employs these equations and provides a means of obtaining a detailed qualitative solution at any location in the flowfield, something that experimental procedures do not offer due to the limited capability of the instrumentation. The resultant flowfield analysis can be inspected at any cross section and along any surface. Local and global properties can be monitored. Parameters that influence flow conditions can be studied and their effects understood. In the present study, injection rates, injection velocity, injection angle, and geometry effects are studied to determine their effects on film cooling.

Grid Generation

The computational grids used in this study are generated using the GRIDGEN program.[9] This program runs on a Silicon Graphics Iris workstation and is used to generate two-dimensional surface grids. Three grids are generated, one for each of the three different slot heights. An additional grid is constructed for the zero secondary flow analysis by changing

the boundary conditions on the grid corresponding to the 3.12-mm slot height. Grid points are clustered near each of the surfaces to increase the resolution in the boundary layer and are also clustered in the secondary and primary mixing regions where density and pressure gradients are high. Each of the grids uses a grid density of 100×100 grid lines, resulting in a total of 10,000 grid points. The grid corresponding to the 4.57-mm step height is illustrated in Fig. 2a.

A grid resolution study is conducted to verify the numerical accuracy of the solutions. An alternate grid is generated corresponding to the 6.07-mm step height geometry. This grid has 50 additional grid lines in both the vertical and horizontal directions, resulting in a grid density of 150×150 or 22,500 grid points. These additional grid points are strategically located along the surface to be film cooled downstream from the injection point. The 50 additional vertical grid lines are added downstream of the mixing plane providing increased clustering behind the splitter-plate base. The 50 horizontal grid lines provide increased clustering along the film-cooled surface. The result is a horizontal grid-spacing reduction of 0.5 and a vertical grid-spacing reduction of 0.025 near the flat surface. The modified grid is illustrated in Fig. 2b.

An additional CFD analysis is conducted using the 150×150 grid and boundary conditions identical to those for CFD run 3 from Table 3. The static temperature distribution on the film-cooled surface for the two analyses are compared and shown in Fig. 3. The comparison indicates that the more dense grid has a temperature distribution 0.2–1.0% higher than the original 10,000 grid point solution. The dense grid solution also had a 0.3% increase in the secondary-to-primary weight flow ratio, which would contribute to the higher surface temperatures. From this grid sensitivity study, it was concluded that a grid density of 100×100 is sufficient and that an increased grid density did not significantly alter the results.

Computational Algorithm

The HAWK2D CFD code is a flowfield simulation computer program based on the strong conservation law form of the Navier-Stokes equations. The basic physics of the code embodies the divergence form of the time-dependent continuity, momentum, and energy equations. These time-dependent equations are solved until steady-state conditions are reached. The perfect gas equation of state and Sutherland's viscosity law are used. Thermodynamic and kinematic properties of a fluid flow are calculated at discrete points within the flow, based on a specified boundary geometry and appropriate flow conditions on these boundaries. Inviscid and viscous flows can be calculated. Viscous flows can be laminar or turbulent and can be treated as fully viscous or as shear-layer flows.

The HAWK2D code is a derivative of the PARC2D code,[10] which was derived from the ARC code. Several modifications have been made to the PARC2D code resulting in the HAWK2D code. One of the modifications involved replacement of the Baldwin and Lomax turbulence model used in

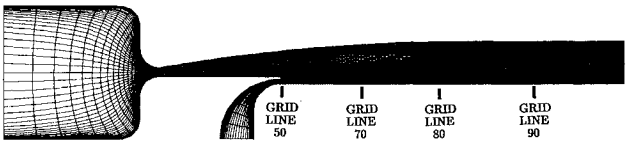

Fig. 2a Computational grid (100×100), 10,000 grid points and grid line identification for convergence monitoring.

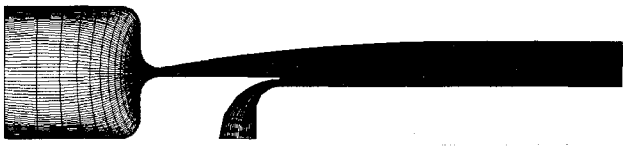

Fig. 2b Computational grid (150×150), 22,500 grid points.

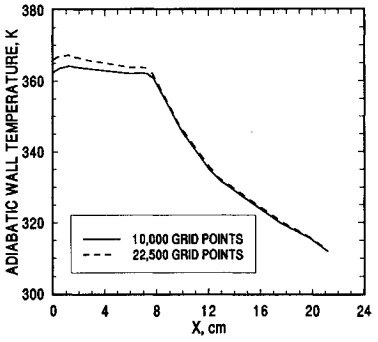

Fig. 3 Adiabatic wall temperature comparison between 10,000 point grid and 22,500 point grid.

PARC2D with a two-equation k-kl turbulence model.[11] The two-equation model is derived from a Reynolds stress closure model and modified for compressible flows.[12] This model is a fully turbulent model and requires no laminar transition. It accounts for viscous dissipation and compressiblity, which is required for a film-cooling effectiveness study.

The artificial dissipation technique in HAWK2D is also different than that in its parent code PARC2D. Smoothing in HAWK2D is implemented separately for each coordinate direction. In the boundary layer, natural viscosity provides sufficient smoothing for numerical stability; therefore, the need for artificial smoothing in the boundary layer is reduced.

The Beam and Warming[13] approximate factorization algorithm is the heart of the computational procedure employed by HAWK2D. The algorithm solves equations produced by central differencing of the Navier-Stokes equations on a regular grid. This algorithm employs the alternating direction implicit (ADI) style formulation to reduce computational time. Variable, spatial, and temporal time steps are used for improved algorithm efficiency and robustness.

Boundary Conditions

The flowfields are represented in a computational domain: that is, each point in the physical domain is represented by a point in computational space. Boundary conditions are assigned to each of the physical boundaries and are represented in computational space. The primary and secondary in-flow planes are specified by a subsonic in-flow boundary condition. Total pressure and temperature along with flow direction are specified on these boundaries. Static pressure and other flowfield quantities are calculated as the solution progresses. The exit plane of the test article uses a supersonic outflow boundary condition, and the flowfield properties at this station are determined by extrapolation from upstream values.

All physical surfaces are modeled as no-slip (viscous flow), adiabatic wall (perfectly insulated) surfaces. The ability to measure or define an adiabatic temperature distribution is very important in the calculation of film-cooling effectiveness. All velocity components and the normal gradients of temperature and pressure are set to zero on these surfaces. Static temperature and pressure are extrapolated from the grid point adjacent to the surface.

The 20 CFD analyses are conducted on a Silicon Graphics Iris workstation. Each of the solutions required approximately 12,000 iterations for convergence. Several flowfield properties can be monitored to determine when a solution converges. Convergence of local flowfield properties such as surface temperature and pressure generally require more computational time than do convergence of global flowfield properties such as mass flow. In general, convergence is usually monitored using a global residual of the conservation variables. Because the current study focuses on local adiabatic surface temperatures, and this temperature is a more conservative convergence parameter than the residual, this parameter was monitored to determine solution convergence.

The adiabatic wall temperature was monitored at four different axial locations along the surface to be film cooled. Grid line numbers corresponding to these locations are specified. Grid line 50 is located at the mixing plane and grid lines 70, 80, and 90 are located farther downstream from the slot; see Fig. 2a. It was observed that the local adiabatic wall temperature converges (approaches a steady-state value) at a slower rate as the distance downstream from the mixing plane is increased. Convergence takes approximately 3,000, 4,500, 7,000, and 11,000 iterations[14] at the location corresponding to grid lines 50, 70, 80, and 90, respectively. As the flow proceeds downstream from the injection point, mixing increases between the primary and secondary streams and more computational time is required to resolve the flowfield.

Data Reduction and Discussion of Results

Computational Fluid Dynamics Comparison with Test Data

A comparison is made between predicted computational data and experimental data. Two different flow conditions corresponding to the 4.57-mm step height geometry are used for the comparison. These flow conditions most closely modeled test conditions available for comparison. Table 4 identifies parameters for each of the two conditions. The secondary-to-primary mass velocity ratio M, secondary-to-primary total temperature ratio TR, and secondary slot Mach number Ma_s are listed. The secondary slot Mach number is a height-averaged value across the exit plane of the slot. A percentage difference between the CFD and test value for each parameter is also included. For each comparison, the local wall adiabatic-to-primary total temperature ratio is plotted against axial distance downstream from the slot X.

The temperature ratio for comparison 1 is shown in Fig. 4. The trends for this case show excellent agreement. At the slot, a downstream distance of zero, both the CFD and test data indicate a temperature ratio of 1.23. At 2.5 cm downstream from the slot, the rate at which the temperature ratio drops increases rapidly for both the CFD and test data due to turbulent mixing between the two streams. As the downstream distance is increased beyond 5 cm, the data asymptotically approach a temperature ratio representative of the mixed temperature between the two streams. The CFD predicted data approach a value 2.3% higher than the test data, indicating a predicted local adiabatic wall temperature higher than the measured temperature. The mass velocity ratio of the CFD analysis is 17% higher than the test mass velocity ratio. This represents an increased amount of heated secondary airflow and therefore would provide improved insulation. In addition, the accuracy of the test measurements is ± 5%. As previously discussed, the test apparatus used can affect the test measurements if the surface of interest is not perfectly insulated.

Table 4 Computational fluid dynamics (CFD) vs test data

	Comparison 1			Comparison 2		
Parameter	CFD	Test	% Dev.	CFD	Test	% Dev.
M	0.075	0.064	17.0	0.038	0.036	6.2
TR	1.233	1.231	0.1	1.233	1.190	3.4
Ma_s	0.360	0.480	33.0	0.230	0.300	23.4

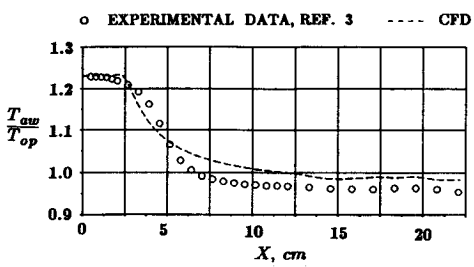

Fig. 4 CFD and test data comparison, H = 4.57 mm and M = 0.038.

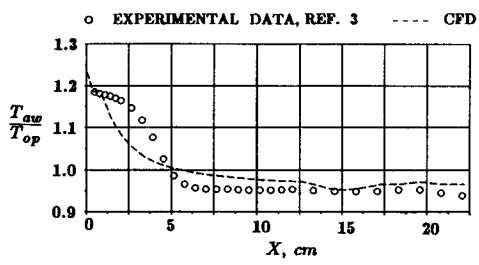

Fig. 5 CFD and test data comparison, H = 4.57 mm and M = 0.075.

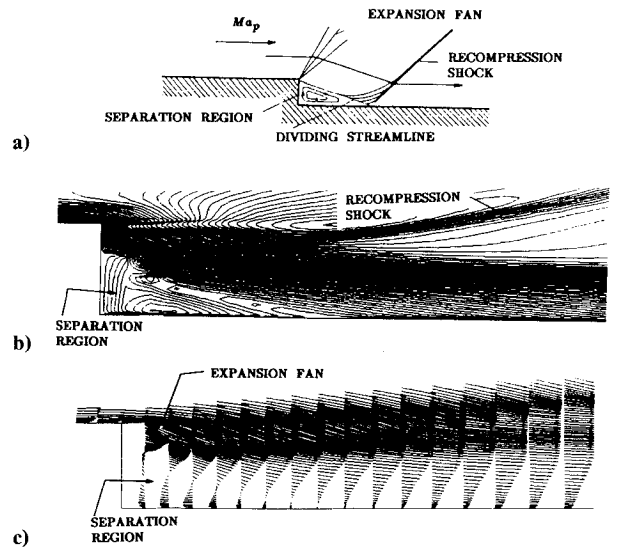

Fig. 6 Supersonic flow characteristics near a step: a) theoretical flow definition; b) CFD Mach contours; c) CFD velocity vectors.

Comparison 2 is illustrated in Fig. 5. This comparison more closely matches the mass velocity ratio and slot Mach number between CFD and test data; however, the total temperature ratio percentage difference increases to 3.4%. The corresponding adiabatic-wall-to-primary-flow temperature ratio data indicate this temperature difference. Immediately downstream of the slot there is a larger difference in the CFD and test data than for the preceding comparison. This indicates the sensitivity of film cooling to the temperature ratio between the two streams. Temperature differences result in density differences. As two streams merge together, mixing increases as the density ratio between the two streams increases. As the downstream distance is increased, both sets of data again asymptotically approach a steady-state value. Given the differences in the parameter values used to make these comparisons, the difficulties in measuring adiabatic wall temperature distributions, and noting the accuracy range of the test instrumentation used, the CFD data compare well with the test data.

Generalized Flowfield Description

Film cooling is affected by the flow conditions existing near the surface of interest. The flowfield of interest in this particular study is supersonic. Knowledge of the flowfield characteristics is helpful in understanding the data obtained and the resultant film cooling effectiveness.

First, consider supersonic flow around a solid step where zero secondary flow is injected. For the geometry under consideration, Fig. 1, primary flow expands downstream from the throat to a Mach number of 2.24 at the mixing plane. At this location, an abrupt solid step is encountered and the primary flow expands around the corner. Figure 6a illustrates the flow characteristics in the neighborhood of this corner. A portion of the primary flow turns downward away from the bulk of the primary flow through an expansion fan. As flow turns

through this expansion fan, it encounters a flat wall. A recompression shock forms and the flow encounters this shock wave and is turned back parallel to the wall. Just downstream of the step and upstream of the recompression shock, a separation zone exists and flow recirculation is present.

This portion of the flowfield as predicted by CFD for the zero secondary flow solution has been magnified in the region of the step and is illustrated in Figs. 6b and 6c. Flow recirculation and the recompression shock are easily detected in these figures. Close inspection of Fig. 6c, which illustrates velocity vectors, identifies flow expansion around the corner and flow recompression downstream of the step where the velocity vectors are turned back parallel to the wall. The recompression shock goes on to impinge on the upper surface of the geometry and is reflected downward. The reflected shock travels downstream and impinges again on the lower surface. This shock pattern can influence the pressure and adiabatic temperature distributions on the lower surface. A more in-depth discussion on the characteristics and flowfield properties of expansion fans and shock waves can be found in Ref. 15.

Now consider the case where the secondary fluid is injected through a slot at the location of the step, Fig. 7. The following discussion draws heavily from that given in Ref. 3. The boundary layer for the primary flow starts at point O′ and for

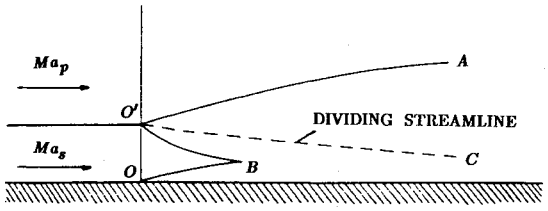

Fig. 7 Flow characteristics of two merging parallel streams.

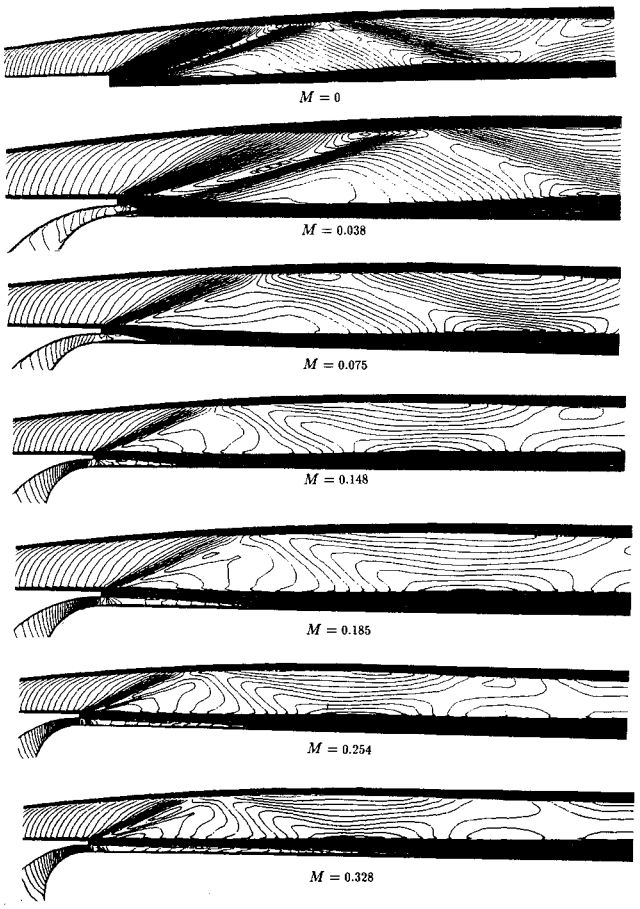

Fig. 8 Flowfield Mach contours (CFD schlieren) for 4.57-mm step.

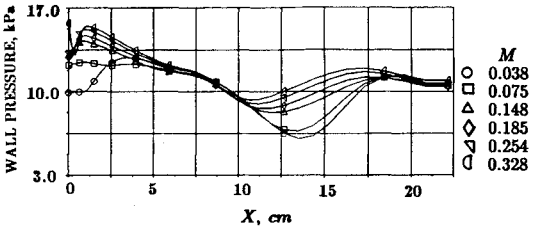

Fig. 9 Surface pressure distribution downstream of the injection point.

the secondary flow at point O. A mixing shear layer between the primary and secondary flowstreams occurs in the region A-O′-B. Only secondary flow exists in region O′-B-O, and no mixing between the two streams occurs. A streamline that theoretically divides the primary stream from the secondary stream is indicated by line O′-C. In the actual flow, turbulent mixing between the two streams causes fluid particles to travel across this streamline.

As the secondary airflow rate is increased, more energy and momentum are contained in the secondary flow stream and point B moves downstream. The secondary flow region O′-B-O remains isolated from the primary stream farther downstream from the injection point, providing improved cooling effectiveness. To illustrate this, CFD produced Mach number contours of the flowfield corresponding to the 4.57-mm step height geometry are shown in Fig. 8. Seven solutions providing secondary-to-primary mass velocity ratios between zero and 0.33 are illustrated.

For the zero secondary flow case, $M = 0$, flow expansion around the corner can be seen and a recompression shock originating just downstream of the step is evident. As discussed previously, this shock travels downstream and impinges on the upper surface, then is reflected downstream and impinges on the lower surface. Although the resolution in this particular illustration does not provide flow details just downstream of the step, it does show that no mixing layer or secondary flow stream is present.

The next six illustrations in Fig. 8 correspond to increasing secondary airflow rates. For the mass velocity ratio $M = 0.038$, the secondary flow region O′-B-O, see Fig. 7, projects just downstream from the injection point. As secondary airflow increases further, this region extends farther downstream and is evident in the figure. The unmixed secondary air flow region provides an insulating film along the surface reducing the convective heat transfer rate between the primary flow and the surface. Film-cooling effectiveness therefore increases. Note that, as more secondary airflow is delivered through the slot, the primary flow turns through a smaller angle around the corner, resulting in reduced expansion around the corner. The recompression shock completely disappears at a mass velocity ratio between 0.038 and 0.075 because the primary flow expansion fan weakens due to increased secondary flow. The disappearance of this shock structure allows the insulating film to continue farther downstream along the surface. At some distance downstream from the injection point, the effects of friction with the lower surface and shear interaction between the primary and secondary streams cause a reduction in momentum of the secondary stream. At this point, the effects of turbulent mixing between the two streams increase and the insulating film breaks down. The film-cooling effectiveness decreases rapidly in this region. Figure 8 compares well with experimental results in Ref. 3.

Pressure Distributions

Local surface pressure distributions downstream of the mixing plane or slot are plotted for the 4.57-mm step height, Fig. 9. The pressure distributions correspond to mass velocity ratio values between 0.038 and 0.328. In this environment, the primary stream flow is expanding and a favorable pressure

gradient exists downstream of the mixing plane. At the location of the slot, there is a significant difference between the absolute wall pressures for each of the mass velocity ratios. These differences are primarily the result of varying secondary supply total pressure (see Table 2); however, local flowfield characteristics particular to each flow rate also influence the surface pressure. The pressure distribution corresponding to $M = 0.038$ increases from 10.3 to 12.4 kPa between 12.5 and 25 mm downstream from the slot. This is due to the recompression shock previously discussed. In this region, distributions for all other values of M decrease because the shock is weaker or does not exist. For all values of M, the pressure distributions are about the same and decrease due to the favorable pressure gradient between a distance of 40 and 110 mm downstream from the slot. Between 110 and 180 mm, the pressures differ for all values of M due to the reflected shock from the upper surface and the expansion of the primary flow. Downstream from this point, the pressure distributions are similar. These pressure distributions compare well with those given in Ref. 3.

Film-Cooling Effectiveness

Most film-cooling studies emphasize the measurement of adiabatic wall temperature distributions. This parameter is very difficult to measure and is significant in the theoretical definition of film-cooling effectiveness because it is the critical value a surface temperature can obtain. To determine how well a surface is being insulated, accurate temperature measurements on the surface are essential. A possible area of concern for experimental studies is that, although the heat flux through a particular surface can approach zero, it is impossible to perfectly insulate a surface. Results can be misleading depending on the quality of the test apparatus. Instrumentation inaccuracy also comes into account. The computational tools used in this study allow an adiabatic boundary condition to be set on the surface of interest. Zero heat flux through the surface is allowed, and a true adiabatic temperature distribution is obtained. By the definition of the adiabatic wall, conduction through the wall is absent. In addition, for the temperature range considered in this study, radiation effects are insignificant; therefore, radiation and conduction on the surface of interest are not being accounted for.

For the current study, the film-cooling effectiveness is defined as

$$\eta = \frac{T_{aw} - T_r}{T_{aw2} - T_r} \tag{1}$$

where T_{aw} is the adiabatic wall temperature and T_{aw2} is its value at the point of secondary fluid injection. The adiabatic wall temperatures are obtained by analyzing each of the three slot-height conditions with varying mass velocity ratio values. The recovery temperature used for all calculations, T_r, is obtained by analyzing the geometry having a step height of 4.57 mm with zero secondary flow. Employing this definition results in an effectiveness parameter that is dependent only on the primary and secondary flows, and the local axial position on the film-cooled surface.

At low primary flow velocities, viscous dissipation and compressibility effects can be neglected. However, the flow environment for the current study is supersonic, and the primary flow velocity is high; these effects cannot be overlooked. A measure of the viscous dissipation and the effects of fluid compressibility is given by the recovery factor r. The recovery temperature T_r is related to the recovery factor[7] r, by the equation:

$$r = \frac{T_r - T_\infty}{T_{op} - T_\infty} \tag{2}$$

where T_{op} is the total temperature of the primary flow, and T_∞ is the local static temperature of the primary flow. This relation applies to viscous, compressible flows. The temperature difference $T_r - T_\infty$ is a measure of the rate of viscous dissipation in the compressible boundary layer. If the recovery temperature T_r and primary flow static temperature are equal, then no dissipation exists. The amount at which T_r increases above T_∞ depends only on the fluid and its velocity. The recovery factor can be approximated by the following relations for laminar and turbulent flows[7]:

$$\text{laminar} \Rightarrow r \simeq Pr^{1/2} \tag{3}$$

$$\text{turbulent} \Rightarrow r \simeq Pr^{1/3} \tag{4}$$

$$\text{Prandtl number} \Rightarrow Pr = \mu C_p / k \tag{5}$$

The Prandtl number is the ratio of the fluid kinematic viscosity to the fluid thermal diffusivity, a number that characterizes the fluids ability to transport momentum more readily than heat ($Pr > 1$) or heat more readily than momentum ($Pr < 1$).

Figure 10 illustrates the recovery factor [Eq. (2)] on the surface of interest for the current study. The data are shown on this expanded scale to illustrate the effect of the expansion fan and reflected shock on the wall surface temperature. These data correspond to the zero secondary airflow analysis conducted on the 4.57-mm step height, Fig. 8, $M = 0$. Just downstream of the injection point, where the flow is separated, the values of the recovery factor are higher than expected. This can be attributed to flow recirculation in this region. At a downstream distance of 12.7 mm, the recovery factor decreases to a value around 0.89, which indicates a decreased wall temperature as the result of the expansion fan. At downstream distances beyond 17.5 cm, the recovery factor increases to approximately 0.91 as the flow travels through the reflected shock wave. The value of 0.91 is higher than that expected for turbulent flow and could possibly be influenced by the exit plane boundary condition.

Mass Velocity Ratio Effect

Figure 11 shows how a variation of the secondary-to-primary mass velocity ratio parameter M affects the cooling effectiveness η. A plot for the 4.57-mm step height is shown. The film-cooling effectiveness is plotted against the axial distance downstream from the injection point or slot for values of M between $M = 0.038$ and 0.328. Recall that the secondary-to-primary temperature ratio is 1.23 and the primary stream Mach number at the mixing plane is 2.24 for each of the analyses.

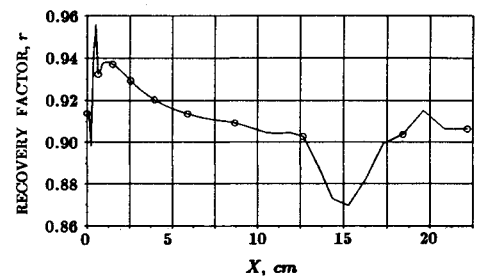

Fig. 10 Recovery factor for $H = 4.57$-mm step, $M = 0$.

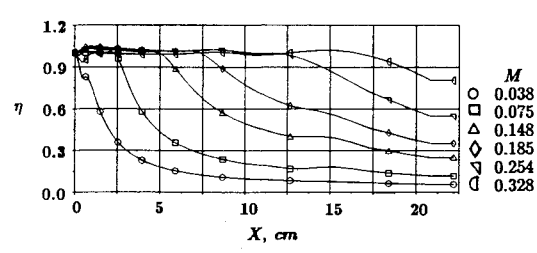

Fig. 11 Mass velocity ratio effect on film-cooling effectiveness.

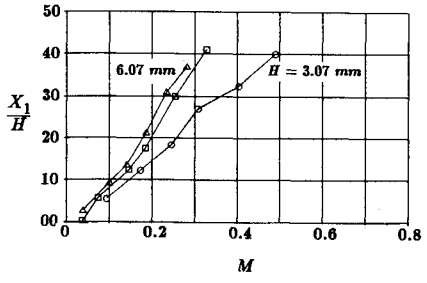

Fig. 12 Dimensionless distance, X_1/H, for near ideal film-cooling effectiveness when $\eta > 0.95$.

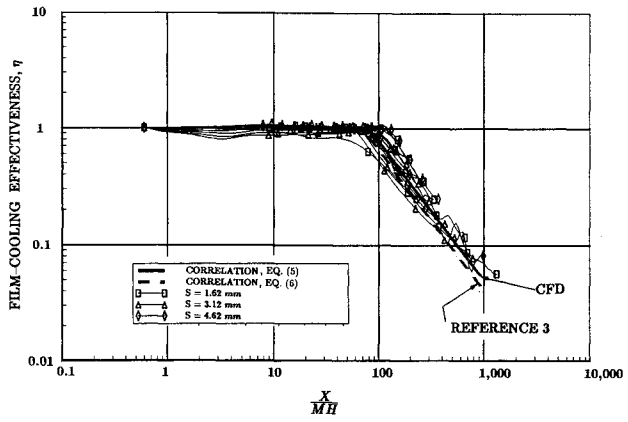

Fig. 13 Film-cooling effectiveness data correlations and comparison with experimental data.

Several points can be made about the indicated trends. At the mixing plane, a distance downstream of zero, the effectiveness value is approximately 1 for each of the mass velocity ratios [see Eq. (1)]. The cooling effectiveness remains close to unity farther downstream as the mass velocity ratio increases. For each of the individual M curves, the effectiveness drops off from a value close to 1 at the indicated downstream distance and asymptotically approaches some value of film-cooling effectiveness depending on the mixed temperature of the two flow streams. The rate at which the effectiveness value drops along a constant value of mass velocity ratio depends on the interaction of heat energy and momentum exchange due to turbulent mixing between the secondary and primary streams.

The distance downstream from the slot for which the effectiveness is within 5% of unity was calculated and is designated X_1. Figure 12 shows a nondimensional length parameter X_1/H plotted against the mass velocity ratio M, where H represents the step height. Three sets of data are shown, one for each step height. It is seen that close to ideal film cooling is maintained farther downstream as the value of M is increased. A second point is that, at a fixed value of M, close to ideal cooling exists farther downstream as step height increases. This can be attributed to the larger separation zone downstream from the mixing plane. The primary flow must travel a farther distance to penetrate down to the surface.

Film-Cooling Correlation

For the specified conditions of this study, it was concluded that Eq. (1) would provide an adequate parameter for data correlation. The data presented in Ref. 14 and in the preceding section could be used for specific cases having similar conditions; however, for convenience, the data is presented on a log-log graph so that a power relationship can be developed. Because of the dependence on the mass velocity ratio M and the downstream axial location X, it is convenient to plot the effectiveness against a parameter containing these variables. In addition, the step height H influences the flow conditions along the surface of interest; it, too, was included in the correlation.

Figure 13 illustrates the results of this study. The film-cooling effectiveness, Eq. (1), is plotted against the correlating parameter X/HM. It is seen that plotting the data against X/HM on a log-log graph collapses the data. A power relationship is derived representing the declining part of the curve. The relationship found to provide the best fit of data is

$$\eta = 180.0 \left(\frac{X}{HM}\right)^{-1.186} \tag{6}$$

The bold straight line shown in Fig. 13 is generated using this relationship. Recall that the definition used for the film-cooling effectiveness η employed the recovery temperature. The tabulated data plotted are from Ref. 14. To show the comparison with the correlation obtained from experimental work, Eq. (7) from Ref. 3

$$\eta = 160.0 \left(\frac{X}{HM}\right)^{-1.2} \tag{7}$$

is represented by a dashed line in in Fig. 13.

The scatter band of data is relatively small but can be significant from a required secondary airflow standpoint. This scatter band is attributed to the different mass velocity ratios analyzed, the secondary flow injection angle at the mixing plane, and the resultant flowfield due to the varying step heights.

The data generally fall onto two straight-line segments. The portion of the film-cooling effectiveness data that are close to unity form one of these lines. The other straight-line section represents a reduction in film-cooling effectiveness due to turbulent mixing. For the two correlations, the declining portion of each curve has the same slope. The difference between the correlations is the value of X/HM at which they decrease from unity. This portion of the curves begins at X/HM values between 70 and 100 and extends out to values of 1000. The value of X/HM at which the data decline from unity for the computational correlation Eq. (6) correspond to the data presented in Fig. 13, which indicate the downstream distance for which the effectiveness is close to unity. In general, there is good agreement between the two correlations. The differences in the point at which the effectiveness drops from unity could result from instrumentation, the insulating capability of the test article, and the computational model.

The correlations indicate that the effectiveness is a function of X/HM; however, because the dissipation and compressibility terms in the energy equation are influenced by M, the effectiveness, Eq. (1), also should depend on $T_{aw2} - T_r$. Goldstein et al.[3] used isoenergetic formulation of the effectiveness to reduce this influence. Isoenergetic film-cooling data were obtained[3] when both primary and secondary flows have the same total temperature. They replace T_r in the numerator of Eq. (1) by the isoenergetic temperature and T_r in the denominator by isoenergetic temperature at the point of injection. Except for the effect of temperature-dependent thermophysical properties, the correlation that uses isoenergetic temperature eliminates the influence of dissipation and compressibility terms in the energy equation. Additionally, when $T_{aw2} - T_r$ is large, the contribution of the dissipation and compressibility terms will be reduced, and the effectiveness correlation given by Eq. (6) approaches the Goldstein et al.[3] data, Eq. (7). For this reason, a relatively large value of $T_{aw2} - T_r = 69°C$ is used in CFD computations.

Conclusions and Recommendations

The computational tools used in this study provide accurate predictions of film-cooling effectiveness and adiabatic temperature distributions. Comparisons with test data were within the accuracy range of the data with which the results were

compared. This indicates that the CFD computations of film cooling in supersonic flow is possible.

The results obtained from this computational study indicate that film cooling through a rearward-facing slot into a supersonic flow stream can be effective. Cooling effectiveness remains close to unity some distance downstream from the injection point. It was indicated[3] that this distance is relatively large for supersonic primary flows due to creation of a separating region in the supersonic environment. At some downstream location, the cooling effectiveness drops due to mixing between the primary and secondary streams. The rate at which the effectiveness decreases is greater than that for subsonic primary flow conditions.[3] Mixing plane geometry affects supersonic flow conditions, which in turn can affect surface insulating. For a given value of M, it was found that the cooling effectiveness was not dependent on the step or slot height for effectiveness values less than 0.95.

The defined correlation, Eq. (6), will provide an approximate value of effectiveness for the specified correlating parameter X/HM. For improved accuracy, the raw data generated should be used and is given in Ref. 14. It is emphasized that this data base be applied only to the range of flow conditions given in Tables 1-3. In addition, because of the dependence on the secondary injection angle, it is recommended that this data base and correlation be used only for the geometric conditions corresponding to tangential secondary flow injection, where the secondary and primary flow streams are parallel.

Acknowledgment

The authors are grateful for computational support at the General Dynamics, Fort Worth Division.

References

[1]Seban, R. A., Chan, H. W., and Scesa, S., "Heat Transfer to a Turbulent Boundary Layer Downstream of an Injection Slot," American Society of Mechanical Engineers, Paper 57-A-36, 1957.

[2]Eckert, E. R. G., and Livingood, J. N. B., "Comparison of Effectiveness of Convection-, Transpiration-, and Film-Cooling Methods with Air as Coolant," NACA Rept. 1182, 1954.

[3]Goldstein, R. J., Eckert, E. R. G., Tsou, F. K., and Haji-Sheikh, A., "Film-Cooling with Air and Helium Injection Through a Rearward-Facing Slot into a Supersonic Airflow," Univ. of Minnesota, Heat Transfer Lab., TR 60, Minneapolis, MN, Feb. 1965.

[4]Seban, R. A., and Back, L. H., "Velocity and Temperature Profiles in a Wall Jet," *International Journal of Heat and Mass Transfer,* Vol. 3, No. 4, 1961, pp. 255-265.

[5]Kacker, S. C., and Whitelaw, J. H., "The Effect of Slot Height and Slot-Turbulence Intensity on the Effectiveness of the Uniform Density, Two-Dimensional Wall Jet," *Journal of Heat Transfer,* Vol. 90, No. 4, 1968, pp. 469-475.

[6]Kacker, S. C., and Whitelaw, J. H., "Prediction of Wall-Jet and Wall-Wake Flows," *Journal of Mechanical Engineering Science,* Vol. 12, No. 6, 1970, pp. 404-420.

[7]Eckert, E. R. G., and Drake, R. M., *Analysis of Heat and Mass Transfer,* Hemisphere, New York, 1987, pp. 421-422.

[8]Chapman, D. R., Kuehn, D. M., and Larson, H. K., "Investigation of Separated Flows in Supersonic and Subsonic Streams with Emphasis on the Effect of Transition," NACA Rept. 1356, 1958.

[9]Steinbrenner, J. P., Chawner, J. R., and Fouts, C. L., "Multiple Block Grid Generation in the Interactive Environment," AIAA Paper 90-1602, June 1990.

[10]Cooper, G. K., "The PARC Code: Theory and Usage," Arnold Engineering Development Center, TR AEDC-TR-87-24, Tullahoma, TN, 1987.

[11]Smith, B. R., "The Turbulence and Wall Layer Model for Compressible Flows," AIAA Paper 90-1483, June 1990.

[12]Smith, B. R., "A Wall Layer Model for Use in Reynolds Stress Closure Turbulence Modeling," AIAA Paper 88-3579, July 1988.

[13]Beam, R. M., and Warming, R. F., "An Implicit Finite-Difference Algorithm for Hyperbolic Systems in Conservative Law Form," *Journal of Computational Physics,* Vol. 22, No. 1, 1976, pp. 87-110.

[14]O'Connor, J. P., "A Numerical Study of Film Cooling in Supersonic Flow," M.S. Thesis, University of Texas at Arlington, Arlington, TX, May 1991.

[15]Anderson, J. D., *Modern Compressible Flow: With Historical Perspective,* McGraw-Hill, New York, 1982, pp. 84-113.